Advanced Composite Materials
Publication details, including instructions for authors and subscription information:
http://www.tandfonline.com/loi/tacm20

Damage Growth Analysis in Particle-Reinforced Composite Using Cohesive Element

Akinori Yoshimura [a] & Tomonaga Okabe [b]

[a] Advanced Composite Group, Aerospace Research and Development Directorate (ARD), Japan Aerospace Exploration Agency (JAXA), 6-13-1 Osawa, Mitaka, Tokyo 181-0015, Japan

[b] Department of Aerospace Engineering, Tohoku University, 6-6-01, Aoba-yama, Aoba-ku, Sendai, Miyagi 980-8579, Japan;, Email: okabe@plum.mech.tohoku.ac.jp

Version of record first published: 02 Apr 2012.

To cite this article: Akinori Yoshimura & Tomonaga Okabe (2011): Damage Growth Analysis in Particle-Reinforced Composite Using Cohesive Element, Advanced Composite Materials, 20:6, 569-583

To link to this article: http://dx.doi.org/10.1163/156855111X610406

VSP

Advanced Composite Materials 20 (2011) 569–583

ADVANCED COMPOSITE MATERIALS
brill.nl/acm

Damage Growth Analysis in Particle-Reinforced Composite Using Cohesive Element

Akinori Yoshimura [a] **and Tomonaga Okabe** [b]

[a] Advanced Composite Group, Aerospace Research and Development Directorate (ARD), Japan Aerospace Exploration Agency (JAXA), 6-13-1 Osawa, Mitaka, Tokyo 181-0015, Japan
[b] Department of Aerospace Engineering, Tohoku University, 6-6-01, Aoba-yama, Aoba-ku, Sendai, Miyagi 980-8579, Japan

Received 16 July 2011; accepted 17 August 2011

Abstract
In this paper, a simple numerical analytical method is proposed for simulating crack extension in a particulate-reinforced composite material. The numerical method is based on finite element analysis with the homogenization method, where crack extension is expressed using embedded cohesive elements. We first present the formulation of the numerical model and verify the model's validity by comparing the simulated crack extension with the linear fracture mechanics. Next we simulate damage extension for a composite reinforced with spherical particles. We consider the cracks in the particles and on particle–matrix interfaces. The analytical results reveal the effect of crack extension on the macroscopic material properties of the composite. The particle crack extends unstably and sharply decreases the tangent modulus of the material, irrespective of the initial flaw size. In contrast, the interfacial crack invariably grows stably and decreases the tangent modulus gradually.

Keywords
Composite materials, crack, finite element, micro-mechanics, multiscale modeling, numerical methods

1. Introduction

Particulate reinforced composite materials are used in widely varying industrial fields because of their outstanding processibility and fine material properties. However, as the load increases, damage occurs in the material. The damage includes the cracks in the particles and on the particle–matrix interfaces. Such cracks degrade material properties. Therefore, it is important to understand damage processes from

* To whom correspondence should be addressed. E-mail: okabe@plum.mech.tohoku.ac.jp
Edited by the JSCM

DOI:10.1163/156855111X610406

the occurrence of the microscopic damage to the final catastrophic failure, and the effects of damage on macroscopic material properties.

Traditionally, the material properties of particulate reinforced composite have been analyzed using Eshelby's equivalent inclusion method [1] in conjunction with the Mori-Tanaka mean field concept [2]. However, traditional methods are not able to assess damage such as particle cracking or the debonding of particles from the matrix. Tohgo *et al.* [3–5] proposed an analytical method that combined the traditional method with a concept of the load carrying capacity of the damaged particle. The capacity was calculated using FEA. The damage occurrence was judged by the stress criteria. The method is simple and robust. Moreover, it can easily assess the stochastic distribution of strength of the particles or the interface. However, the method assumes that crack extension is always instantaneous; the crack extension process is therefore neglected. We believe that the crack does not always extend instantaneously because crack extension is affected by conditions such as loading conditions and crack path location. Therefore, it is necessary to establish a method with consideration of the crack extension process in particle-reinforced composite materials.

Herein, we propose a novel numerical simulation method to simulate crack extension in a particle-reinforced composite material. The model is based on a homogenization method [6, 7]. A particle-reinforced composite material can be regarded approximately as a periodic inhomogeneous material. Homogenization method is an analytical method that enables us to obtain the equivalent homogenized material properties merely by analyzing the response of the unit cell of inhomogeneity to the unit strain. To consider crack extension, we introduced cohesive elements to the homogenization method. It has been demonstrated that cohesive elements can simulate the crack extension in the composites using an energy criterion, and that the simulated crack extension is equivalent to linear fracture mechanics [8–12].

This paper is organized as follows. In Section 2, we formulate the analytical method by combining the homogenization method, in which the unit cell contains the cohesive zone. Next, in Section 3, we compare the crack extension calculated using the proposed method to that calculated using linear fracture mechanics in order to verify the validity of the proposed model. Finally, in Section 4, we perform finite element analysis to simulate the crack extension in composites reinforced with spherical particles. The simulation results reveal the relation between the crack extension and the material properties.

2. Formulation

2.1. Cohesive Element

The cohesive zone model (CZM) assumes a cohesive zone around the crack tip, where cohesive traction resists crack opening. Cohesive traction eliminates the stress singularity around the crack tip. Moreover, it can express the crack extension in an energy criterion by considering energy that is consumed by cohesive traction

as a judgment factor. Let $\dot{\mathbf{T}}$ and $\dot{\mathbf{\Delta}}$ denote the rate of the cohesive traction and the rate of the crack opening. The velocity-shape virtual work principle is written as

$$\int_V \dot{\boldsymbol{\sigma}} : \delta\dot{\boldsymbol{\varepsilon}}\, \mathrm{d}V + \int_{S_{\mathrm{coh}}} \dot{\mathbf{T}} \cdot \delta\dot{\mathbf{\Delta}}\, \mathrm{d}S = \int_{S_t} \dot{\mathbf{f}} \cdot \delta\dot{\mathbf{u}}\, \mathrm{d}S, \tag{1}$$

where $\dot{\boldsymbol{\sigma}}$ denotes the rate of Cauchy's stress tensor, $\dot{\boldsymbol{\varepsilon}}$ denotes the strain rate tensor, $\dot{\mathbf{f}}$ denotes external force rate vector, and $\dot{\mathbf{u}}$ denotes the displacement rate vector. This paper describes formulation of small strain problems. The cohesive element is an implementation of the cohesive zone model in the finite element analysis. Cohesive elements are embedded at interfaces of solid elements along a predefined crack path. Cohesive traction is defined as a function of the relative displacement (separation) between the solid elements. In this study, we adopted a Dugdale-type traction-separation relation proposed by Okabe *et al.* [9, 11, 12]. In the Dugdale-type cohesive element, separation was suppressed until the traction satisfied a condition for transition of crack path into the cohesive zone. In this study, we used a penalty spring for suppression of the separation and adopted the maximum traction criterion for the condition for separation. When the tensile or the shear component reached the threshold, the penalty spring was deleted. After the separation, the Dugdale-type cohesive element generated constant cohesive traction independent of the separation distance. Finally, the element was unloaded at one time when the energy that was consumed by the element reached the fracture toughness (Fig. 1). For the mixed mode crack extension, we employed an elliptic mode-mixture rule. When the energy release rates in modes I, II and III are satisfied

$$\left(\frac{G_{\mathrm{I}}}{G_{\mathrm{Ic}}}\right)^2 + \left(\frac{G_{\mathrm{II}}}{G_{\mathrm{IIc}}}\right)^2 + \left(\frac{G_{\mathrm{III}}}{G_{\mathrm{IIIc}}}\right)^2 = 1, \tag{2}$$

the traction was unloaded, where G_{I}, G_{II} and G_{III} respectively denote modes I, II and III energy release rates, and G_{Ic}, G_{IIc} and G_{IIIc}, respectively, denote the fracture toughnesses in modes I, II and III.

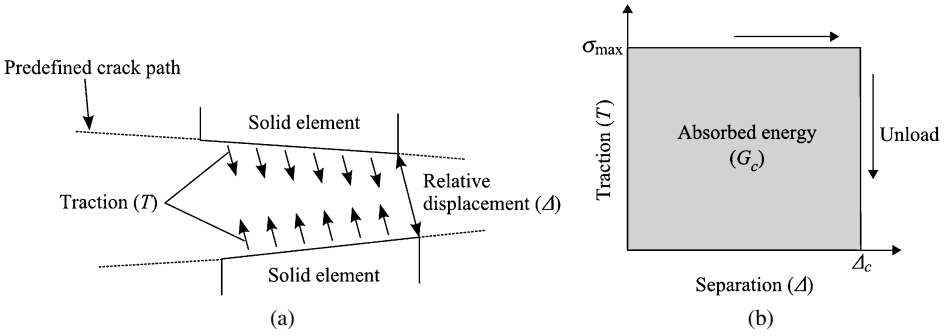

Figure 1. Schematic of the cohesive element. (a) Schematic of a cohesive element. (b) Traction and separation.

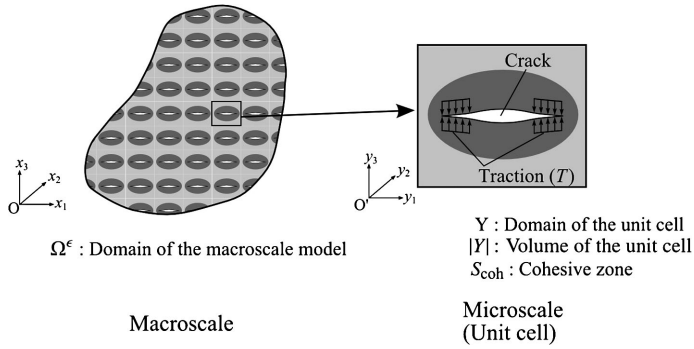

Figure 2. Macroscopic analytical domain Ω^ϵ and microscopic analytical domain (unit cell) Y. The unit cell contains a crack and cohesive zone.

2.2. Homogenization Method

Consider a macroscopic domain Ω^ϵ that includes microscopic periodic inhomogeneity. Let Y denote the unit cell of inhomogeneity. Unit cell Y contains cracks and a cohesive zone (Fig. 2). Let ϵ denote the scale parameter between the macroscopic domain and the unit cell, which is calculated as shown below:

$$\epsilon = \frac{l}{L}. \tag{3}$$

In the equation, L and l, respectively, represent characteristic lengths of the macroscopic domain and the unit cell. We use a coordinate system O–$x_1x_2x_3$ for the macroscopic domain Ω^ϵ; we use another coordinate system O′–$y_1y_2y_3$ for the microscopic domain Y. The x_1, x_2 and x_3 axes and the y_1, y_2 and y_3 axes respectively have the same directions. When components of an arbitrary small vector d$\mathbf{x}$ are written as $(\mathrm{d}x_1, \mathrm{d}x_2, \mathrm{d}x_3)$ using the coordinate system O–$x_1x_2x_3$, they can also be written as

$$\mathrm{d}\mathbf{x} = \left(\frac{1}{\epsilon}\mathrm{d}x_1, \frac{1}{\epsilon}\mathrm{d}x_2, \frac{1}{\epsilon}\mathrm{d}x_3\right) = (\mathrm{d}y_1, \mathrm{d}y_2, \mathrm{d}y_3) \tag{4}$$

using the coordinate system O′–$y_1y_2y_3$.

When the body force is negligible, the velocity-shape equilibrium is

$$\frac{\partial \dot{\sigma}_{ij}^{\epsilon}}{\partial x_i} = 0, \tag{5}$$

where $\dot{\boldsymbol{\sigma}}^\epsilon$ denotes the stress rate tensor. The stress rate tensor can also be written as a bivariable function $\dot{\boldsymbol{\sigma}}$ which has two vector arguments: x and y. Using the bivariable function $\dot{\boldsymbol{\sigma}}$, we can rewrite the equilibrium as

$$\frac{\partial \dot{\sigma}_{ij}}{\partial x_i} + \frac{1}{\epsilon}\frac{\partial \dot{\sigma}_{ij}}{\partial y_i} = 0. \tag{6}$$

Because the macroscopic domain contains numerous unit cells, we consider the limit of the equilibrium equation (6) as ϵ approaches to zero. Consideration of the limit separates the equilibrium into two scale equilibria:

$$\frac{\partial \dot{\sigma}_{ij}}{\partial x_i} = 0 \tag{7}$$

and

$$\frac{\partial \dot{\sigma}_{ij}}{\partial y_i} = 0. \tag{8}$$

We assume that the displacement rate $\dot{\mathbf{u}}$ can be expressed by the summation of macroscopic component $\dot{\mathbf{u}}^0$ and microscopic disturbing component $\epsilon\dot{\mathbf{u}}^1$. The macroscopic component $\dot{\mathbf{u}}^0$ is uniform through the unit cell, but the microscopic disturbance component $\epsilon\dot{\mathbf{u}}^1$ has unit-cell periodicity. When we consider the limit of $\epsilon \to 0$, the strain rate $\dot{\boldsymbol{\varepsilon}}$ is obtained as

$$\dot{\varepsilon}_{ij} = \frac{1}{2}\left(\frac{\partial \dot{u}_i^0}{\partial x_j} + \frac{\partial \dot{u}_j^0}{\partial x_i}\right) + \frac{1}{2}\left(\frac{\partial \dot{u}_i^1}{\partial y_j} + \frac{\partial \dot{u}_j^1}{\partial y_i}\right). \tag{9}$$

The first term on the right-hand side means the macroscopic strain rate; it is denoted by $\dot{\mathbf{E}}$. The constructive equation between the stress rate and the strain rate is written as

$$\dot{\sigma}_{ij} = c_{ijkl}\dot{\varepsilon}_{kl}, \tag{10}$$

where c_{ijkl} denotes the elasticity tensor.

Consideration of the unit-cell integration of dot product of equation (8) with an arbitrary virtual displacement rate vector $\delta\dot{\mathbf{u}}^1$ which has unit cell periodicity gives as

$$\int_Y \frac{\partial \dot{\sigma}_{ij}}{\partial y_i} \delta \dot{u}_j^1 \, \mathrm{d}Y = 0. \tag{11}$$

Applying the Gauss theorem and partial integration for equation (11) with consideration of the symmetry in c_{ijkl} and the uniformity of macroscopic strain rate tensor through the unit cell, we obtain the following:

$$\int_Y c_{ijkl} \frac{\partial \dot{u}_k^1}{\partial y_l} \frac{\partial \delta \dot{u}_j^1}{\delta y_i} \, \mathrm{d}Y = -\dot{E}_{kl} \int_Y c_{ijkl} \frac{\partial \delta \dot{u}_j^1}{\delta y_i} \, \mathrm{d}Y + \int_{\Gamma_y} \dot{\sigma}_{ij} \delta \dot{u}_j^1 n_i \, \mathrm{d}\Gamma + \int_{\Gamma_i} \dot{\sigma}_{ij} \delta \dot{u}_j^1 n_i \, \mathrm{d}\Gamma. \tag{12}$$

Therein, Γ_y represents the boundary of the unit cell, and Γ_i denotes the crack surface and cohesive zone. Applying Cauchy's formula deletes the second term on the right-hand side because the neighboring unit cells are in mutual equilibrium. Moreover, applying Cauchy's formula for the third term on the right-hand side reveals

that the term is equal to the cohesive traction rate on the cohesive zone. Therefore, we can rewrite equation (12) as shown below.

$$\int_Y c_{ijkl} \frac{\partial \dot{u}_k^1}{\partial y_l} \frac{\partial \delta \dot{u}_j^1}{\delta y_i} \, \mathrm{d}Y = -\dot{E}_{kl} \int_Y c_{ijkl} \frac{\partial \delta \dot{u}_j^1}{\delta y_i} \, \mathrm{d}Y - \int_{S_{\mathrm{coh}}} \dot{T}_j \delta \dot{u}_j^1 \, \mathrm{d}S. \tag{13}$$

In fact, equation (13) is the microscale virtual work principle. We use a Dugdale-type cohesive element: cohesive traction rate vector $\dot{T}_i = 0$ through area S_{coh} when equation (2) is not satisfied in any cohesive element in the S_{coh}. In such a case, equation (13) can be rewritten as

$$\int_Y c_{ijkl} \frac{\partial \dot{u}_k^1}{\partial y_l} \frac{\partial \delta \dot{u}_j^1}{\delta y_i} \, \mathrm{d}Y = -\dot{E}_{kl} \int_Y c_{ijkl} \frac{\partial \delta \dot{u}_j^1}{\delta y_i} \, \mathrm{d}Y. \tag{14}$$

We can solve the problem by introducing characteristic displacement χ_i^{kl}, which connects the microscopic displacement rate and macroscopic strain rate as $\dot{u}_i^1 = -\chi_i^{kl} \dot{E}_{kl}$ because equation (14) has the same form as that in the conventional homogenization method. Characteristic displacement χ_i^{kl} is calculable as

$$\int_Y c_{ijpq} \frac{\partial \chi_p^{kl}}{\partial y_q} \frac{\partial \delta \dot{u}_i^1}{\delta y_j} \, \mathrm{d}Y = \int_Y c_{ijkl} \frac{\partial \delta \dot{u}_i^1}{\delta y_j} \, \mathrm{d}Y. \tag{15}$$

Using characteristic displacement χ_i^{kl}, we can obtain macroscopic elasticity tensor C_{ijkl}^H as

$$C_{ijkl}^H = \frac{1}{|Y|} \int_Y \left(c_{ijkl} - c_{ijpq} \frac{\partial \chi_p^{kl}}{\partial y_q} \right) \mathrm{d}Y. \tag{16}$$

On the other hand, if any cohesive element in S_{coh} satisfies equation (2), then the boundary condition must be fixed because unloading must be instantaneous. Therefore, macroscopic strain rate $\dot{E}_{kl}$ must be equal to zero, and equation (13) can be rewritten as presented below:

$$\int_Y c_{ijkl} \frac{\partial \dot{u}_k^1}{\partial y_l} \frac{\partial \delta \dot{u}_j^1}{\delta y_i} \, \mathrm{d}Y = -\int_{S_{\mathrm{coh}}} \dot{T}_j \delta \dot{u}_j^1 \, \mathrm{d}S. \tag{17}$$

In that equation, the right-hand side is the surface force rate. We can easily solve the equation because equation (17) has the same form as that in the conventional finite element analysis. Unloading affects the macroscopic stress. Variation of macroscopic stress $\dot{\mathbf{S}}$ is calculable using the microscopic displacement rate $\dot{\mathbf{u}}^1$ as

$$\dot{S}_{ij} = \frac{1}{|Y|} \int_Y c_{ijkl} \frac{\partial \dot{u}_k^1}{\partial y_l} \, \mathrm{d}Y. \tag{18}$$

The discussion presented above reveals that we can analyze the crack extension in the particulate reinforced composites as follows. When equation (2) is not satisfied in any cohesive element in S_{coh}, we solve equation (15) just as we do using the conventional homogenization method. When equation (2) is satisfied in any cohesive

element, we repeatedly solve equation (16), which is solvable just as conventional finite element analysis is, with fixed macroscopic strain until equation (2) cannot be satisfied in any element.

It is noteworthy that Matouš, Geubelle *et al.* also proposed a numerical model [13, 14] based on the homogenization method and the cohesive zone model. However, we adopted Dugdale-type cohesive elements for the present model. Therefore the simulations were more simple and stable; moreover, we can obtain the homogenized elastic tensor easily by solving equation (16), just as with conventional homogenization analysis.

3. Model Verification

We verified the validity of the numerical method by comparing the numerical results with analytical results calculated using linear fracture mechanics because our numerical method is quite novel. Figure 3 presents a schematic of the three-dimensional finite element model, which represents a unit cell. The unit cell was a cube consisting of the matrix and spherical reinforcement. The cube edge length was 2.2 mm; the reinforcement diameter was 1.0 mm. The volume fraction of the reinforcement was about 0.5%. We assumed, at the center of the model, a circular crack path that was perpendicular to the x-axis. The path is shown as 'crack path of the inclusion crack' in Fig. 3. We introduced a circular initial crack at the center of the model. Four models were prepared, in which the respective radii of the initial cracks were 0.050, 0.125, 0.250 and 0.375 mm. We applied uniform macroscopic tensile stress along the x-axis and calculated the stress, which caused crack extension. For those calculations, the materials of the reinforcement and the matrix were identical.

Material properties and parameters of cohesive elements used in the analysis are presented in Table 1. When uniform tensile stress is applied at infinity to the circular

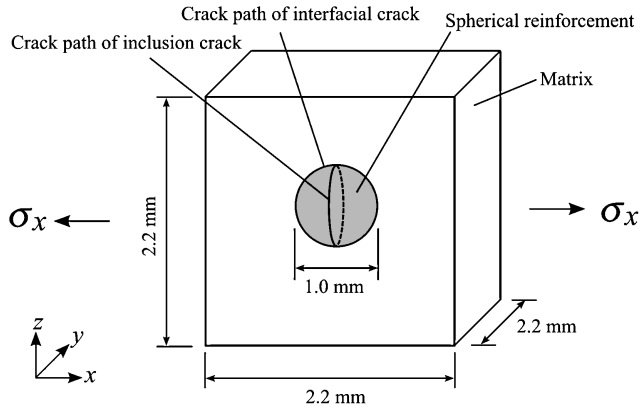

Figure 3. Schematic of the 3D finite element model. The unit cell contains a spherical reinforcement.

Table 1.
Properties of material and cohesive elements used for the simulation performed for comparison with the linear fracture mechanics

(a) Material properties	
Young's modulus, E (GPa)	3.0
Poisson's ratio, ν	0.3
(b) Properties of cohesive elements	
Mode I maximum traction, $\sigma_{\max}$ (MPa)	20.0
Mode II maximum traction, $\tau_{\max}$ (MPa)	40.0
Mode III maximum traction, $\tau_{\max}$ (MPa)	40.0
Mode I fracture toughness, G_{Ic} (J/m^2)	10.0
Mode II fracture toughness, G_{IIc} (J/m^2)	20.0
Mode III fracture toughness, G_{IIIc} (J/m^2)	20.0

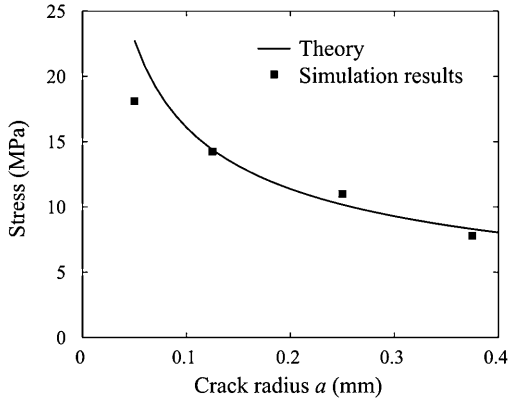

Figure 4. Relation between the crack radius a and the stress causing crack extension.

crack, the radius of which is a, we obtain the stress causing crack extension $\sigma_{\max}$ from linear fracture mechanics [15] as in the equation

$$\sigma_{\max} = \frac{\pi}{2}\sqrt{\frac{G_{\mathrm{Ic}}E}{\pi a}}, \tag{19}$$

where G_{Ic} denotes mode I fracture toughness. Figure 4 depicts the simulation results and the results of equation (19). Numerical simulation results agree well with the analytical results. The causes of the subtle difference were the influence of the cohesive zone and interference with neighboring cracks, which derived from the periodic boundary condition.

The results demonstrate that the numerical model proposed in this paper can express the equivalent crack extension with linear fracture mechanics.

4. Damage Extension Simulation

4.1. Inclusion Crack

We conducted damage extension simulations for the dispersed composite material reinforced by the spherical particle. We used the same finite element model as that used in Section 3 (Fig. 3). It is noteworthy that the present model includes only one spherical particle in a unit cell. Therefore, it is implicitly assumed that the particles are regularly arranged and that the damage state is identical through all the particles in the composite. We adopted the assumption to conduct a detailed investigation of the damage evolution phenomenon. Using the unit cell containing more particles, we can readily conduct more realistic simulations.

First, we simulated the extension of the inclusion crack. The circular crack path, which was perpendicular to the x-axis, was assumed (as indicated by 'crack path of inclusion crack' in Fig. 3). The circular initial crack was introduced at the center of the model. We prepared three models for which the radii of initial cracks r were, respectively, 0.050, 0.125 and 0.250 mm. Macroscopic stress was applied along the x-axis, and inclusion crack extension was simulated.

Table 2 shows the material properties and the parameters of cohesive elements used for the simulation. Irrespective of the radius of initial crack, the inclusion crack extended unstably. The crack extended to the interface between the reinforcement and matrix simultaneously with the beginning of the crack extension. Figure 5 portrays the stress distributions of the unit cell immediately before and immediately after the crack extension. The stress state was almost identical through the crack path except for the vicinity of the initial crack tip immediately before the crack extension occurred. Therefore, once the crack extension occurred, the crack extension condition was satisfied continuously, and the crack extended unstably to the crack

Table 2.
Properties of materials and cohesive elements used in the damage extension simulation

(a) Material properties	
Young's modulus of reinforcement, E_r (GPa)	15.0
Poisson's ratio of reinforcement, ν_r	0.17
Young's modulus of matrix, E_m (GPa)	3.0
Poisson's ratio of matrix, ν_m	0.3
(b) Properties of cohesive elements	
Mode I maximum traction, $\sigma_{\max}$ (MPa)	20.0
Mode II maximum traction, $\tau_{\max}$ (MPa)	40.0
Mode III maximum traction, $\tau_{\max}$ (MPa)	40.0
Mode I fracture toughness, G_{Ic} (J/m^2)	10.0
Mode II fracture toughness, G_{IIc} (J/m^2)	20.0
Mode III fracture toughness, G_{IIIc} (J/m^2)	20.0

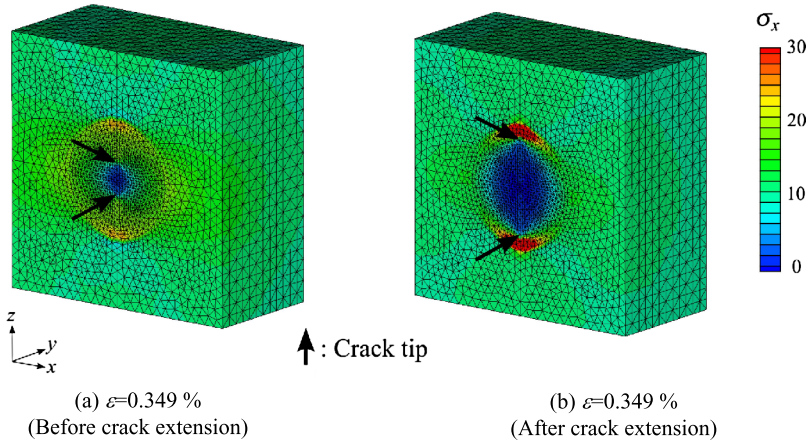

Figure 5. Stress distribution in the unit cell of the inclusion crack model. The initial crack radius r is 0.125 mm. This figure is published in color in the online version.

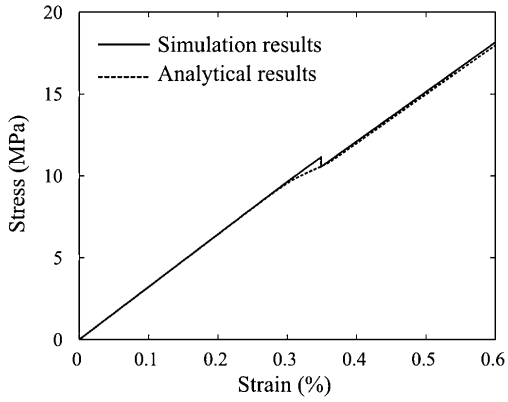

Figure 6. Macroscopic stress–strain relations of the inclusion crack model. The initial crack radius r is 0.125 mm.

path edge. Crack extension greatly decreased the stress carrying capability of the reinforcement.

Figure 6 shows the simulated relation between the macroscopic stress and the macroscopic strain for initial crack radius r of 0.125 mm. The crack extension sharply reduced the macroscopic stress because the crack reduced the stress carrying the reinforcement. Figure 6 also presents a plot of the analytical results of the method proposed by Tohgo and Cho [5], which combines Eshelby's equivalent inclusion method and the results of FEA. For the calculation, the strength of reinforcements was distributed as a Weibull distribution, where shape factor m was 20; the average strength was equal to the average stress of the particle when crack extension occurred in our simulation. Our results agreed well with those obtained using the method presented by Tohgo and Cho because the premise of their method agreed

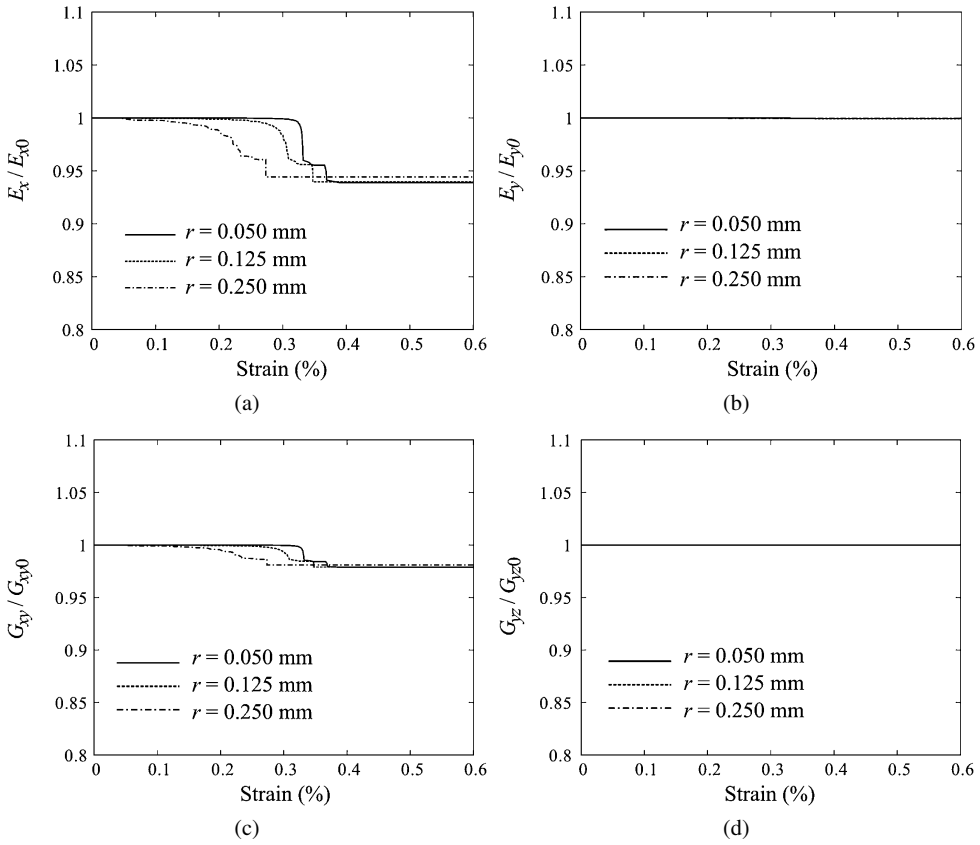

Figure 7. Relations between the macroscopic material properties and macroscopic tensile strain. (a) E_X. (b) E_y. (c) G_{xy}. (d) G_{yz}.

well with the simulation results, in which the crack extended instantaneously when the stress in the reinforcement reached the critical value (strength). The stress–strain relation of the method described by Tohgo and Cho was smooth because the reinforcement strength was distributed according to the Weibull distribution.

Figure 7 presents the calculated macroscopic material properties as functions of the x-direction component of the macroscopic strain. The normal tangent modulus in the x-direction E_x and the shear tangent modulus G_{xy} decreased sharply when the crack extension occurred. However, the crack extension scarcely had an effect on the normal tangent modulus in y-direction E_y and the shear tangent modulus G_{yz} because the crack surface was perpendicular to the x-axis. The following is the reason why the transitions of the properties were affected strongly by the initial flaw size: the crack extended unstably. Therefore the properties changed greatly with the occurrence of the crack extension. The larger initial flaw size decreased the strain which caused the crack extension. Consequently, the transition of the properties occurred at smaller strain when the initial flaw size was larger.

4.2. Interfacial Crack

Next we conducted a crack extension simulation of the interfacial crack between the reinforcement and the matrix. We used the same finite element mesh as that used in Section 4.1. (Fig. 3). The material properties and the parameters of the cohesive elements were also the same as those used in Section 4.1. (Table 2). The crack path was introduced at the interface between the reinforcement and the matrix, which is indicated by 'crack path of interfacial crack' in Fig. 3. The area of the crack path for which the distance from x-axis was smaller than the critical value d was debonded as the initial crack. We prepared three models in which d was, respectively, 0.086, 0.158 and 0.227 mm.

Simulation results revealed that the crack extended stably irrespective of the initial crack size. The simulated stress distributions in the unit cell are presented in Fig. 8. The stress was larger near the x-axis; it became smaller as the distance from the x-axis increased. Once the crack extension condition was satisfied at the crack tip, the crack extended. However, after the crack extension, the stress around the crack tip became less than that immediately before the crack extension. Therefore, the crack extension condition was not satisfied continuously; the crack extended stably. Because the interfacial crack extended, the stress carrying of the reinforcement decreased gradually.

Figure 9 depicts the macroscopic stress–strain relation for d of 0.158 mm. In Fig. 9, the results calculated using the method presented by Tohgo and Cho [5] are also shown. In their method, the shape factor m was 20, and the average strength was equal to the average stress of reinforcement when crack extension started in our simulation. The results of Tohgo and Cho presented strong nonlinear behavior when the crack occurred. In our results, however, weak nonlinear behavior continued to a much higher strain because the premise of the method of Tohgo and Cho, which assumed the crack occurred at the whole interface when the stress reached the critical value, did not agree with our simulation results. The simulation results

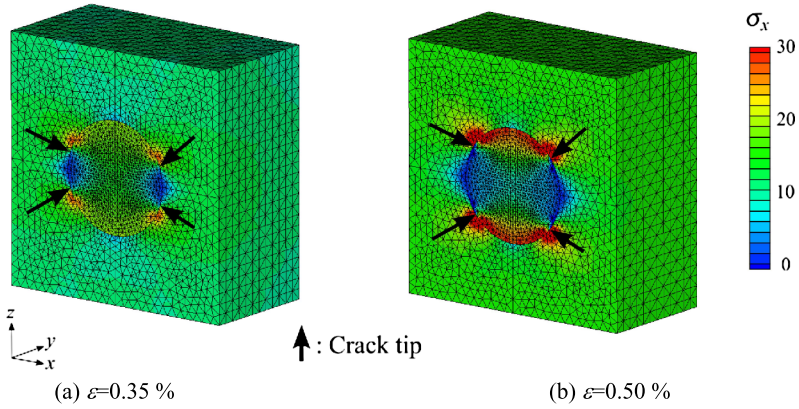

Figure 8. Stress distribution in the unit cell of the interfacial crack model. The radius of initial crack d is 0.158 mm. This figure is published in color in the online version.

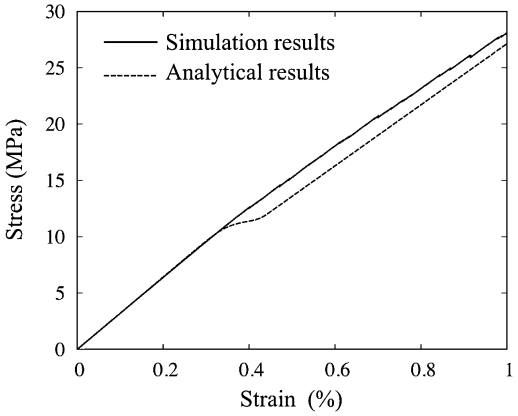

Figure 9. Macroscopic stress–strain relations of the interfacial crack model. The initial crack radius d is 0.158 mm.

demonstrated that it is important to consider the extension process of the crack when we simulate the interfacial crack of the dispersed composite material.

Figure 10 presents the calculated macroscopic material properties as functions of the x-direction component of macroscopic strain. As the strain increased, the tangent moduli decreased in all directions. The normal tangent modulus in x-direction E_x and the shear tangent modulus G_{xy} reduced sharply when the crack extension started; their reduction rate decreased as the strain increased. In contrast, the normal tangent modulus in y-direction E_y and the shear tangent modulus G_{yz} decreased gradually when the crack extension started, but their reduction rate became greater as the strain increased because the crack surface was perpendicular to the x-axis when crack extension started, and the direction of the crack surface gradually approached the direction perpendicular to the y and z axes.

The following is the reason why the decreases of the material properties were scarcely affected by the initial flaw size: the stress, which was greater near the x-axis, lessened as the distance from the x-axis increased. Therefore when the initial flaw size was smaller, the crack extension began at a smaller strain. When the initial flaw size was larger, the crack extension began at larger strain. However, a smaller initial crack began to extend at a smaller strain. In that case, the strain grew larger concomitantly with the crack extension because the crack extended stably. When the crack reached a certain size, the strain was almost equal to the strain that was produced when the initial crack of the certain size began to extend. That is, the crack size at a certain macroscopic strain was almost equal irrespective of the initial crack size. Therefore, the degradation of the material properties did not depend on the initial flaw size: it depended solely on the elastic energy state.

The discussion presented above indicates that the interfacial crack might extend stably in actual composites. It is noteworthy that the results described above might be affected by the crack extension criteria used for this study. The results of other criteria are left as goals of future studies.

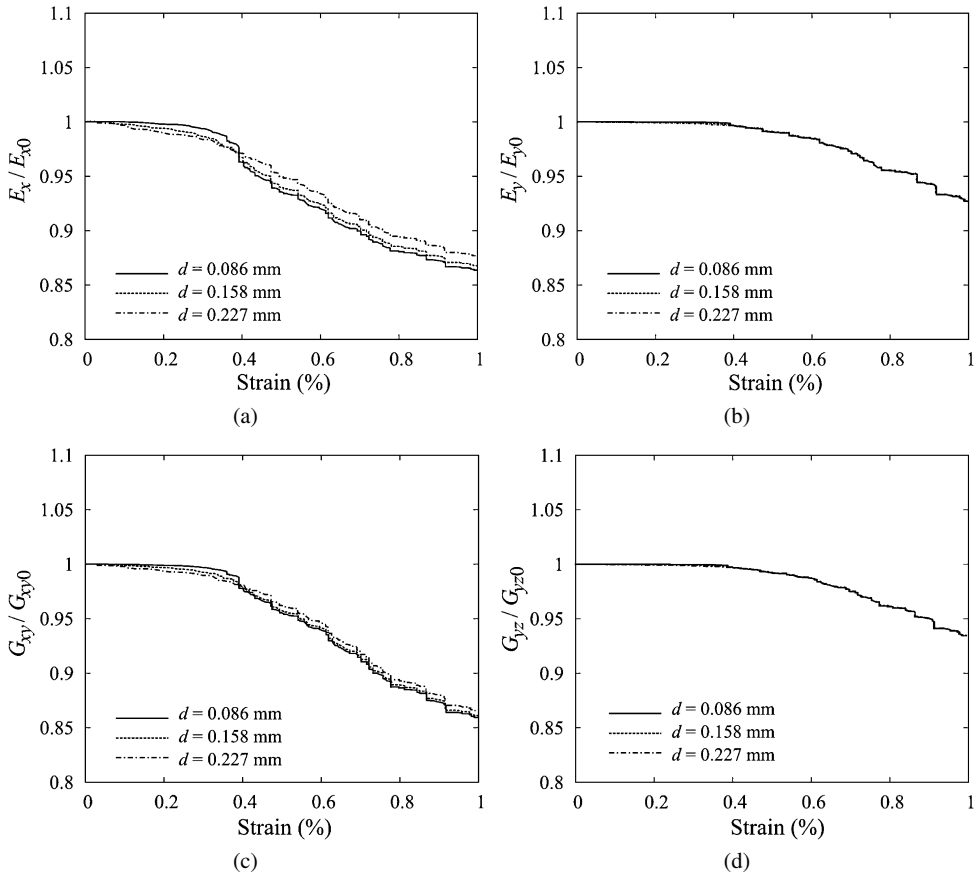

Figure 10. Relation between macroscopic material properties and macroscopic tensile strain. (a) E_x. (b) E_y. (c) G_{xy}. (d) G_{yz}.

5. Conclusion

This paper proposed a simple numerical analytical method for crack extension simulation in the dispersed composite material. The method was based on cohesive elements and the homogenization method. We performed crack extension simulations of the particle-reinforced composite using the proposed method.

1. Comparison between the simulation results obtained using the proposed method and the results of linear fracture mechanics demonstrated that our method can express the equivalent crack extension to that shown by the linear fracture mechanics.

2. Crack extension simulation in the particulate reinforced composite showed that the inclusion crack extended unstably. The results validated the conventional method, which relies on the assumption that the instantaneous evolution of the crack by the stress criteria.

3. Crack extension simulation revealed that the interfacial crack between the reinforcement and the matrix extended stably. The results implied that interfacial cracks might extend stably in actual composites. Therefore, it is necessary to consider the crack extension process when we simulate the interfacial crack. Moreover, decreases of the material properties did not depend on the initial flaw size. However, the effect of the crack extension criteria on the simulation results remains as a subject for future work.

References

1. J. D. Eshelby, The determination of the elastic field of an ellipsoidal inclusion, and related problems, *Proc. Roy. Soc. Lond. Ser A* **A241**, 376–396 (1957).
2. T. Mori and K. Tanaka, Average stress in matrix and average elastic energy of materials with misfitting inclusions, *Acta Metall.* **21**, 571–574 (1973).
3. Y. T. Cho, K. Tohgo and H. Ishii, Finite element analysis of a cracked ellipsoidal inhomogeneity in an infinite body and its load carrying capacity, *Trans. Japan Soc. Mech. Eng. A* **62**, 1903–1909 (1996) (in Japanese).
4. Y. T. Cho, K. Tohgo and H. Ishii, Load carrying capacity of a broken ellipsoidal inhomogeneity, *Acta Mater.* **45**, 4787–4795 (1997).
5. K. Tohgo and Y. T. Cho, Theory of reinforcement damage in discontinuously reinforced composites and its application, *Trans. Japan Soc. Mech. Eng. A* **65**, 514–522 (1999) (in Japanese).
6. K. Terada and N. Kikuchi, *An Introduction to Homogenization*. Maruzen, Tokyo (2003) (in Japanese).
7. D. Cioranescu and P. Donato, *Introduction to Homogenization*. Oxford University Press, New York (1999).
8. P. H. Geubelle and J. S. Baylor, Impact-induced delamination of composites: a 2D simulation, *Compos. B* **29**, 589–602 (1998).
9. T. Okabe, M. Nishikawa and N. Takeda, Numerical simulation of tensile damage evolution in FRP cross-ply laminates, *Trans. Japan Soc. Mech. Eng. A* **72**, 1254–1261 (2006) (in Japanese).
10. A. Yoshimura, S. Yashiro, T. Okabe and N. Takeda, Characterization of tensile damage progress in stitched CFRP laminates, *Adv. Compos. Mater.* **16**, 223–244 (2007).
11. M. Nishikawa, T. Okabe and N. Takeda, Numerical simulation of interlaminar damage propagation in CFRP cross-ply laminates under transverse loading, *Int. J. Solids Struct.* **44**, 3101–3113 (2007).
12. M. Nishikawa, T. Okabe and N. Takeda, Determination of interface properties from experiments on the fragmentation process in single-fiber composites, *Mater. Sci. Eng. A* **480**, 549–557 (2008).
13. K. Matouš and P. H. Geubelle, Multiscale modelling of particle debonding in reinforced elastomers subjected to finite deformations, *Int. J. Numer. Methods Eng.* **65**, 190–223 (2006).
14. H. M. Inglis, P. H. Geubelle, K. Matouš, H. Tan and Y. Huang, Cohesive modeling of dewetting in particulate composites: micromechanics *vs.* multiscale finite element analysis, *Mech. Mater.* **39**, 580–595 (2007).
15. H. Okamura, *An Introduction to the Linear Fracture Mechanics*. Baihukan, Tokyo (1976) (in Japanese).